538.21

MAGNETOPLASMA WAVES IN BISMUTH

V. S. EDEL'MAN

Institute of Physics Problems, USSR Academy of Sciences

Usp. Fiz. Nauk 102, 55-85 (September, 1970)

1. INTRODUCTION

1.1. Calculations Based on a Simple Model

INVESTIGATIONS of the propagation of undamped electromagnetic waves in metals at frequencies below the plasma value have been going on now for a decade (the first paper on bismuth[1] appeared in 1961) and many characteristic features of this phenomenon are established knowledge.

We can distinguish two cases, depending on the ratio of the numbers of free electrons and holes in a metal or a semiconductor.* If $N_e \neq N_h$, low-frequency "helicon" waves are observed and their spectrum is $\omega^2 \propto k^2(\mathbf{k}\cdot\mathbf{H})^2$. If $N_e = N_h$, the range of existence of undamped waves shifts into the microwave range and the spectrum of these waves in strong magnetic fields becomes $\omega \propto kH$, which is formally identical with the spectrum of magnetohydrodynamic waves in a gaseous plasma.[3] In pure metals, the condition for $N_e = N_h$ is an even number of electrons per unit cell of the lattice[4] and therefore this situation is not exceptional and the propagation of waves in such a case is of general interest.

A simple calculation demonstrates the possibility of the existence, in a metal in a magnetic field, of waves with a large damping length, under conditions in which the densities of the carriers are $N_e = N_h$ and their spectra are isotropic and quadratic. We shall assume that the field $\mathbf{E}$ in a metal varies in accordance with the law $\mathbf{E} = \mathbf{E}_0\exp[i(\mathbf{k}\cdot\mathbf{r} - \omega t)]$. We shall neglect the collision processes ($\omega\tau \gg 1$) and use a linear approximation in $\mathbf{E}$ to consider the motion of carriers in a static field $\mathbf{H}$ such that $\Omega_{e,h} \gg \omega$. For the sake of simplicity, we shall assume that $d_{e,h} \ll \lambda = 2\pi/k$. Having determined, from the Lorentz equation, a correction to the carrier velocity, we shall use the relationship $\mathbf{j} = \sigma\mathbf{E} = e(N_h\delta\mathbf{v}_h - N_e\delta\mathbf{v}_e)$ to find the conductivity tensor

$$\sigma = \begin{Vmatrix} -i\omega c^2H^{-2}(N_hm_h+N_em_e); & 0; & 0; \\ 0; & -i\omega c^2H^{-2}(N_hm_h+N_em_e); & 0; \\ 0; & 0; & ie^2\omega^{-1}(N_h/m_h+N_e/m_e) \end{Vmatrix}. \quad (1)$$

If we ignore the displacement current (i.e., if we assume $\omega \ll \omega_{p1}$), we find that Maxwell's equations give*

$$\mathbf{j} = ic^2[\mathbf{k}\,[\mathbf{kE}]]/4\pi\omega.$$

Neglecting the term $(ic^2/4\pi\omega)(k_yk_z/\sigma_{zz}) \approx (\omega/\Omega)^2$, we obtain the dispersion equation

$$[\sigma_{xx} + (ic^2k^2/4\pi\omega)]\,[\sigma_{yy} + (ic^2k^2\cos^2\vartheta/4\pi\omega)]\,[\sigma_{zz} + (ic^2k^2\sin^2\vartheta/4\pi\omega)] = 0. \quad (2)$$

This equation has two real solutions

$$k_S = \omega H^{-1}[4\pi(N_hm_h + N_em_e)]^{1/2},$$
$$k_P = \omega H^{-1}\cos^{-1}\vartheta\,[4\pi(N_hm_h + N_em_e)]^{1/2} \quad (3)$$

which represent the propagation of two waves at different velocities. One of them (the S wave) is polarized perpendicularly to the plane containing the vectors $\mathbf{H}$ and $\mathbf{k}$, whereas the other (the P wave) is polarized in that plane.

An allowance for the relaxation processes results in the damping of a wave. The damping can be calculated by replacing ω in σ_{ik} with $\omega + (i/\tau)$ and representing k as $k' + ik''$ (k' and k'' are real numbers). Simple calculations show that $k''/k' = 1/2\omega\tau$.[5]

For most metals, $N \approx 10^{22}$ cm^{-3}, $m \approx m_0$ and an estimate of k in a field $\sim 10^4$ Oe for $\omega \approx 6\times10^{10}$ sec^{-1} (corresponding to a wavelength of 3 cm in vacuum) yields $k \approx 6\times10^4$ cm^{-1}. For $\omega\tau \approx 10^2$, the damping length of a wave is $\sim 3\times10^{-3}$ cm. It follows that such waves can be investigated only in very thin, high-quality single crystals or in much stronger fields ($\sim 10^6$ Oe).

The carrier density in some metals is anomalously low. These metals include arsenic, antimony, bismuth, and graphite: the lowest carrier densities ($\sim 10^{17}$ cm^{-3}) and small effective masses ($\sim 0.1\ m_0$) are encountered in bismuth and graphite. However, it is difficult to prepare high-quality graphite crystals and the currently available crystals of graphite are much inferior to those of bismuth in respect of the duration of the relaxation time. Therefore, bismuth is preferred for investigations.

The results of the calculations show that the assumptions made to obtain these results can be satisfied experimentally in the case of bismuth. Let us assume that $H \approx 10$ kOe and $\omega \approx 6\times10^{10}$ sec^{-1}. Using the properties of bismuth, $N = 3\times10^{17}$ cm^{-3}, $m \approx 0.2\ m_0$, we obtain $\omega/\Omega < 0.1$, $\omega/\omega_{p1} \approx 6\times10^{10}/10^{14} < 10^{-3}$. The wave vector is $k \approx 2\times10^2$ cm^{-3} and the wavelength is $\lambda \approx 3\times10^{-2}$ cm. In the field $H = 10$ kOe, the maximum diameter of an electron orbit in bismuth is $d \approx 6\times10^{-5}$ cm, i.e., $d/\lambda \approx 2\times10^{-3}$. The relaxation time is $\tau \approx 10^{-9}$ sec (see Sec. 3.3). Hence, we find that $k''/k' \approx 10^{-2}$ and the waves are weakly damped. These considerations show that bismuth is a suitable material for the investigation of plasma phenomena in compensated metals. They also show why bismuth is, so far, practically the only metal in which plasma effects have been investigated.

1.2. High-frequency Conductivity Tensor

The results of experiments, particularly those performed under the conditions described by $\omega \approx \Omega$ and $d \approx \lambda$, can be understood and analyzed in detail provided the calculations are rigorous and an allowance

*For details, see the review by Kaner and Skobov. [2]

*$[\mathbf{k}[\mathbf{kE}]] \equiv \mathbf{k}\times[\mathbf{k}\times\mathbf{E}]$.

is made for the anisotropy of the energy spectrum of the carriers and for the dispersion in time and space. The rigorous theory cannot be given here in full, but the reader is referred to the review by Kaner and Skobov.[2] We shall simply give the expression for the conductivity tensor[6], which we shall use later:

$$\sigma_{lk}=\frac{e^2}{2\pi^2\hbar^3}\sum_{e,\,h}\int_{-p_{z_0}}^{p_{z_0}}\frac{dp_z m}{\Omega}\sum_n\frac{\overline{v_l^{-n}(-\psi)\,v_k^n(\psi)}}{in-[i(\omega-k_z\bar{v}_z)/\Omega]}. \tag{4}$$

The first summation is carried out over all parts of the Fermi surface

$$\psi=\int^{\varphi}(\mathbf{kv}-k_z\bar{v}_z)\,d\varphi',\quad \varphi=eHt/mc,$$

and $v_k^n(\psi)$ is the n-th Fourier component of the expansion of the function $v_k(\varphi)\exp[i\psi(\varphi)/\Omega]$. In strong fields, we can expand σ_{lk} in terms of ω/Ω, $\mathbf{k}\cdot\mathbf{v}/\Omega$, $\psi/\Omega \approx \mathbf{k}\cdot\mathbf{v}/\Omega$ ($\mathbf{k}\cdot\mathbf{v}/\Omega \approx d/\lambda$), and $k_z\bar{v}_z/\omega$, which gives the following expressions:[6]

$$\sigma_{zz}=\frac{e^2}{2\pi^2\hbar^3}\frac{i}{\omega}\int dp_z m\bar{v}_i^2,$$

$$\sigma_{z\alpha}=-\sigma_{\alpha z}=\frac{e^2}{2\pi^2\hbar^3}\int\frac{dp_z}{\Omega}\begin{cases}\overline{-v_z(p_y-\bar{p}_y)}, & \alpha=x,\\ \overline{v_z(p_x-\bar{p}_x)}, & \alpha=y,\end{cases} \tag{5}$$

$$\sigma_{\alpha\beta}=\sigma_{\beta\alpha}=-\frac{ie^2\omega}{2\pi^2\hbar^3}\int\frac{dp_z}{m\Omega^2}\begin{cases}\overline{(p_y-\bar{p}_y)^2}, & \alpha=\beta=x,\\ \overline{(p_x-\bar{p}_x)^2}, & \alpha=\beta=y,\\ \overline{-(p_x-\bar{p}_x)(p_y-\bar{p}_y)}, & \alpha=x,\ \beta=y.\end{cases}$$

If the carrier spectrum is quadratic and isotropic, the expressions in Eq. (5) reduce to the components of Eq. (1).

1.3. Fermi Surface of Bismuth

We shall be constantly referring to the Fermi surface of bismuth (Fig. 1). We recall[7] that it consists of one hole and three electron surfaces, which are nearly ellipsoidal.* The conductivity tensor of Eqs. (4) and (5) can be calculated if we know the velocities, momenta, and effective masses simply at the Fermi level. Therefore, ignoring the deviation of the Fermi surface from the ellipsoidal shape, we shall assume that the energy spectra of the carriers in bismuth can be represented as follows. The spectrum of holes is

$$2\varepsilon_h=\frac{p_1^2}{M_1}+\frac{p_2^2}{M_2}+\frac{p_z^2}{M_3}, \tag{6}$$

and that for one of the electron ellipsoids (principal axes are used), is

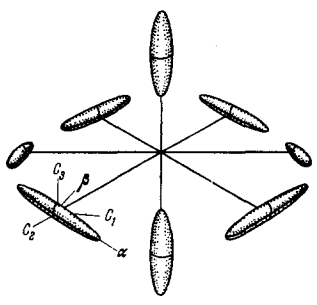

FIG. 1. Model of the Fermi surface of bismuth.

*The ellipsoids are located at the boundaries of a Brillouin zone, and there are six electron semiellipsoids and two hole semiellipsoids per each zone. The system of ellipsoids shown in Fig. 1 includes also parts of the Fermi surface in the adjacent Brillouin zones.

$$2\varepsilon_e=\frac{p_\alpha^2}{m_\alpha}+\frac{p_\beta^2}{m_\beta}+\frac{p_2^2}{m_2}; \tag{7}$$

the other two ellipsoids are rotated by $\pm 120^\circ$ about the C_3 trigonal axis. In these expressions, the various parameters are:[8] $2\epsilon_h = 3.75\times10^{-14}$ erg, $M_1 = M_2 = 0.063\ m_0$, $M_3 = 0.65\ m_0$, $2\epsilon_e = 5.78\times10^{-14}$ erg, $m_\alpha = 1.27\ m_0$, $m_\beta = 1.15\times10^{-2}\ m_0$, $m_2 = 0.57\times10^{-2}\ m_0$. The major axis ($\alpha$) of each of the electron ellipsoids is inclined at an angle of $6^\circ20'$ with respect to the basal plane.

1.4. Model Calculation of the Wave Velocity

The wave velocity in all the cases of interest to us can be calculated using Eqs. (4)—(7) and the dispersion equation, whose general form is

$$\|\sigma_{lk}+[ic^2/4\pi\omega(k^2\delta_{lk}-k_lk_k]\|=0, \tag{8}$$

By way of example, we shall calculate the asymptotic value of the wave velocity (i.e., the velocity in the limit of strong fields) for $\mathbf{H}\parallel C_1$, $\mathbf{k}\parallel C_2$. Using symmetry considerations, we can easily show that $\sigma_{12}(1) = \sigma_{21}(1) = \sigma_{32}(1) = \sigma_{23}(1) \equiv 0$. The value of $\sigma_{13}(1)$ is not zero but its appearance is associated with the slight inclination of the electron ellipsoids with respect to the basal plane. The value of this component is proportional to the square of this angle, and can be ignored because it does not exceed 1%. Thus, only the diagonal terms remain in the conductivity tensor and the dispersion equation (8) gives

$$k^2=4\pi\omega\sigma_{33}(1)/ic^2. \tag{9}$$

This solution represents an undamped wave with $\mathbf{E}\parallel C_3$ (the solution $k^2 = 4\pi\omega\sigma_{11}(1)/ic^2$ corresponds to a damped wave).

Using Eq. (6) and the Lorentz equation, we find the quantities which determine the contribution of the holes to $\sigma_{33}(1)$:

$$p_{z_0}=p_1=(2\varepsilon_hM_1)^{1/2},\quad m=\frac{1}{2\pi}\frac{\partial S}{\partial\varepsilon}=\frac{1}{2\pi}\frac{\partial(\pi p_2p_3)}{\partial\varepsilon}=(M_2M_3)^{1/2};$$
$$p_y=p_{y_0}\cos\varphi,\quad p_{y_0}^2=M_2[2\varepsilon_h-(p_z^2/M_1)]=2\varepsilon_hM_2[1-(p_z^2/p_{z_0}^2)];$$
$$\bar{p}_y=0,\quad \overline{(p_y-\bar{p}_y)^2}=\overline{p_y^2}=p_{y_0}^2/2.$$

Substituting these values into the integral of the expression for σ_{xx} given in Eq. (5), we obtain

$$\sigma_{33}^h(1)=-(i/3)(c^2\omega/\pi^2\hbar^3H^2)(2\varepsilon_h)^{3/2}M_1^2M_3^{1/2}. \tag{10}$$

Similar calculations for electrons and summation over all three ellipsoids give

$$\sigma_{33}^e(1)=-i(6c^2\omega/\pi^2\hbar^3H^2)(2\varepsilon_e)^{3/2}m_\alpha^{1/2}m_\beta^{1/2}m_2^{3/2}. \tag{11}$$

Equations (9)—(11) represent the solution of our problem.

Calculations similar to those in the present section can be carried out for any directions of H and k. However, the treatment becomes quite complex in the case of asymmetrical directions of H and k because the nondiagonal terms must be included and the analysis becomes much more cumbersome.

The numerical results of calculations of the wave velocity for symmetrical directions of H and k are given in Table I.

Table I. Velocity of magnetoplasma waves in bismuth[8]

Direction of H	Direction of k	Direction of E	vH^{-1} (exper.), 10^{-4} cm/sec	vH^{-1} (calc.), 10^{-4} cm/sec
C_3	C_3	C_1 or C_2	3.05±0.05	2.93±0.15
	C_1	C_2	2.75±0.05	
	C_2	C_1	3.1±0.15	
C_2	C_2	C_3	2.40±0.1	2.50±0.1
	C_2	C_1	1.90±0.05	2.07±0.08
	C_3	C_1	1.87±0.05	2.12±0.08
	C_3	C_2	2.73±0.1 *)	2.45±0.1 *)
	C_1	C_3	2.30±0.05	2.45±0.1
C_1	C_3	C_2	1.99±0.05	2.12±0.08
	C_3	C_1	5.5±0.2 *)	6.09±0.15 *)
	C_2	C_3	6.15±0.15	6.09±0.15
	C_2	C_1	1.9±0.1 *)	1.9±0.08 *)

*Values of $vH^{-1}/\cos\vartheta$, obtained for H inclined at 7-10° to the axis listed in the first column. The calculated values refer to H parallel to that axis.

2. EXPERIMENTAL INVESTIGATIONS

2.1. Experimental Technique

The working frequency f in wave investigations is governed by the need to make the damping as weak as possible, i.e., we should satisfy $\omega\tau \gg 1$, which limits us to frequencies $f \gtrsim 1$ GHz. Some of the experiments have been carried out at frequencies ranging from $\sim 10^8$ Hz[9] to ~600 GHz[10] but most of the measurements have been made in the frequency range 10–20 GHz because of the technical advantages, which include the thorough knowledge of this frequency range, the possibility of using moderate magnetic fields (~10 kOe or less), and the reasonably high value of $\omega\tau \approx 10$–100.

The propagation of such waves makes the metal transparent and alters its surface impedance. Therefore, these waves can be investigated using the standard methods for recording changes in the Q factor and in the natural frequency of a resonator containing a sample (for example,[11]); or the methods for recording a microwave signal transmitted by a sample.[12] Figure 2 shows one of the simple circuits, whose sensitivity ($\Delta R/R \sim 10^{-4}$) is sufficient for most of the investigations of the wave properties. This circuit works satisfactorily over a wide dynamic range of the Q factor.

A signal from a klystron, modulated at a frequency of ~1 kHz, passes through a resonator (containing a sample), a detector, and a narrow-band amplifier, from which it is fed to a peak detector, which selects a signal of frequency 12 Hz, the modulation frequency of the magnetic field (additional electromagnet coils are used for this purpose). This signal is passed to a second narrow-band amplifier and then on to a phase-sensitive detector. It is plotted as the Y coordinate by an automatic recorder. The X coordinate is the voltage from a Hall probe placed in the gap of the electromagnet. If the resonator is coupled weakly to the transmission line, the signal intensity is proportional to the square of the Q factor of the resonator ($T \propto Q^2$), and the circuit records the value of dT/dH. Experiments show that Q is governed primarily by the surface impedance of bismuth and, therefore, the recorded quantity is $dR^{-2}/dH = R^{-3}dR/dH$.

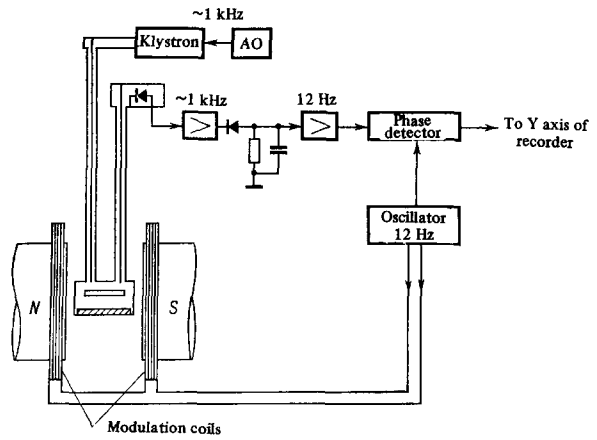

FIG. 2. Apparatus used to investigate the properties of magnetoplasma waves. [13] AO is an audiofrequency oscillator.

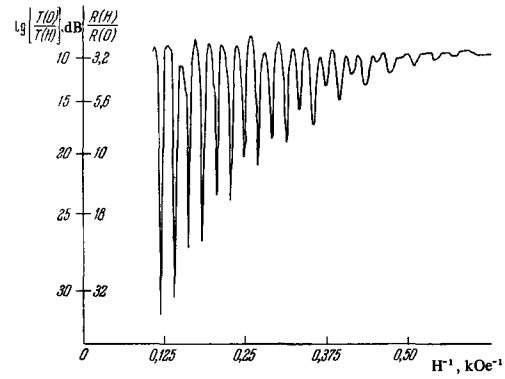

FIG. 3. Oscillations of the high-frequency surface impedance of bismuth, caused by the excitation of standing waves. [15] $k \parallel C_3$, $H \parallel C_2 \parallel E$, $\vartheta = -13°$, f = 9.60 GHz, D = 0.47 mm, T = 1.5°K.

A strip resonator can be used conveniently in the frequency range 10–20 GHz[11] It has the advantages of a small size, large space factor, and linear polarization of high-frequency currents so that waves of different polarizations can be studied separately.

The samples being investigated should be single crystals characterized by a large value of the mean free path of carriers. Good results are obtained using samples grown in demountable quartz moulds.[14] The value of τ for such samples can reach $\sim 4 \times 10^{-9}$ sec (at T = 0°K). Samples are usually in the form of disks of 18 mm diameter and are 0.2–2 mm thick.

2.2. Experimentally Observed Oscillations

A part of a microwave incident on a metal penetrates below the surface and excites magnetoplasma waves. Since the wave velocity is $v \ll c$, the vector k in the metal is directed along the normal to the surface, irrespective of the angle of incidence of the wave (if the sample is the wall of a resonator, its surface is a constant phase plane, which corresponds to an angle of incidence equal to $\pi/2$). Magnetoplasma waves travelling within a plane-parallel plate are reflected by the surfaces and interfere, so that if

$$n\lambda/2 = D \qquad (12)$$

and the wave damping is weak, Fabry-Perot resonances

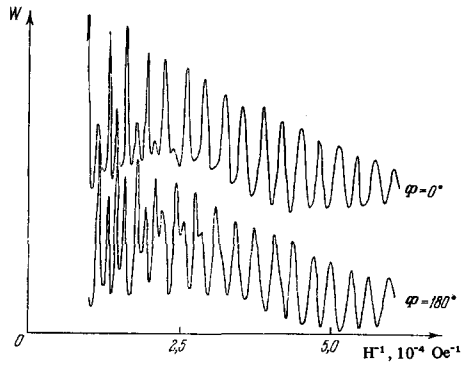

FIG. 4. Oscillations of the power of microwaves which have traversed a single crystal of bismuth. These oscillations are associated with the excitation of Rayleigh resonances. [15] The additional peaks, located between the principal maxima, are due to Fabry-Perot resonances which appear in strong fields. $\mathbf{k} \parallel C_3$, $\mathbf{H} \perp C_1 \parallel \mathbf{E}$, $\vartheta = 68°$, f = 8.85 GHz, D = 1.0 mm, T = 1.5°K. Φ is the phase of the reference signal reaching the detector simultaneously with the measured signal.

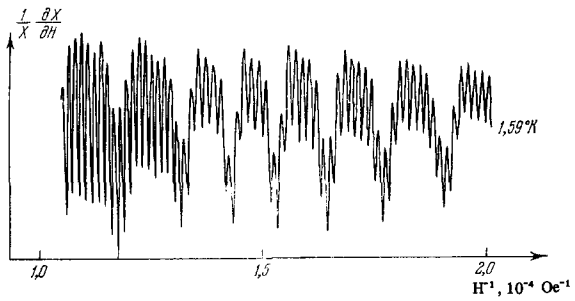

FIG. 5. Oscillations of the high-frequency impedance of a bismuth single crystal, associated with the excitation of Rayleigh resonances. The long-period oscillations are associated with waves propagated at right-angles to the plane of the disk-shaped sample in the case $\mathbf{k} \parallel C_3 \parallel \mathbf{N}$. The short-period oscillations are associated with the waves propagated parallel to the flat surfaces of the sample in the case $\mathbf{k} \perp \mathbf{N}$. $\mathbf{H} \parallel C_2 \parallel \mathbf{E}$ for the flat surfaces, f = 9.5 GHz, D = 1.75 mm, 17.8 mm diameter, T = 1.6°K.

are excited.[6] The wave velocity depends on the applied magnetic field and, therefore, when the magnetic field is reduced gradually, the condition of Eq. (12) is satisfied periodically, which leads to resonances of the surface impedance (absorption maxima shown in Fig. 3) and resonances of the transparency (transmission maxima shown in Fig. 4). When the magnetic field intensity is reduced, the wavelength decreases, the damping in the bulk of a sample increases, and the resonances broaden into sinusoidal oscillations (Fig. 3).[5]

Rayleigh resonances may also be observed in the transmission pattern. They are due to the interference between the signal transmitted through a sample and the signal which passes outside the sample. The periodicity of these resonances is given by the condition

$$n\lambda = D, \tag{13}$$

i.e., these resonances are half as frequent as the Fabry-Perot resonances (Fig. 4). One can use as a reference signal the stray microwave power leaking across the contacts between a sample and the resonator (or the waveguide) to the end of the sample outside the resonator.[12] Such stray leakage gives rise to Rayleigh resonances in investigations of the surface impedance. These resonances are manifested in Fig. 3 by differences of the amplitude of the even and odd oscillations.

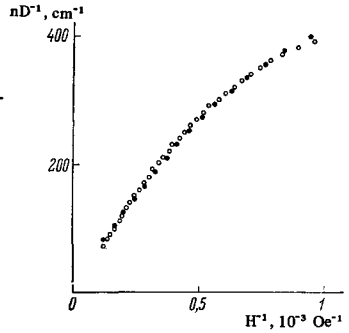

FIG. 6. Dependence of the resonance order n, divided by the thickness of the sample D, on the value of H^{-1}. [15] $\mathbf{H} \parallel \mathbf{k} \parallel C_3$, f = 9.35 GHz. ○) D = 0.47 mm; ●) D = 1.00 mm.

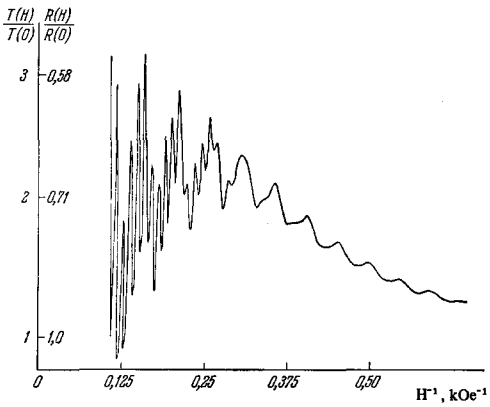

FIG. 7. Oscillations of the high-frequency impedance of bismuth showing the simultaneous excitation of two types of wave: the long-period oscillations are associated with the S waves and the short-period ones with the P waves. [15] $\mathbf{k} \parallel C_3$, $\mathbf{H} \perp C_1$, $\vartheta = 80°$, $\mathbf{E} \parallel C_2$, f = 9.53 GHz, D = 0.47 mm, T = 1.5°K.

In addition to the resonances considered so far, other types of oscillation may be observed. Thus, disk-shaped samples, 17.8 mm in diameter and 1.74-2 mm, thick may exhibit oscillations associated with the propagation of waves parallel to the surface plane (Fig. 5). These oscillations are excited by stray currents flowing across the ends of the sample. Their periodicity is given by the condition (13), where D is now the diameter of the sample.

3. PROPERTIES OF WAVES IN STRONG FIELDS

3.1. Oscillations of the surface impedance of bismuth (Fig. 3) and of its transparency (Fig. 4) have been observed experimentally. The relevant experiments show that weakly damped electromagnetic waves can indeed propagate in bismuth. An additional proof of the relationship between oscillations and wave processes in a metal is provided by experiments on samples of various thicknesses. In Eq. (12), the wavelength λ is a function only of H and ω. Therefore, if H and ω are fixed, we should observe $n_1 D_1^{-1} = n_2 D_2^{-1}$ for samples of different thicknesses D_1 and D_2; this relationship has been confirmed experimentally (Fig. 6).

The relationship governing the oscillation period $D\Delta H^{-1}|_{H,\omega} = \text{const}$ can be deduced quite easily from two values of n differing by unity in Eq. (12) and from the definition of the derivative.

3.2. We shall now consider how far the theory describes the behavior of the waves in question. We shall consider the asymptotic case of strong fields in which there is no dispersion.

The principal conclusion of the theory—the presence of weakly damped waves—has been proved experimentally. The possibility of the simultaneous existence of two waves (S and P) with different velocities given by Eq. (3) is confirmed for the case of bismuth by the oscillations shown in Fig. 7 (the oscillations of two periods appear simultaneously) and by the observations of waves of different velocities when the polarization of E is varied (Table I).

For the S waves, we have $\mathbf{E} \parallel [\mathbf{H} \times \mathbf{k}]$; and for the P waves, we have $\mathbf{E} \parallel [\mathbf{H} \times [\mathbf{H} \times \mathbf{k}]]$. These are the polarizations which correspond to the best conditions for the observation of the S and P oscillations.[6,15]

We shall now consider some quantitative relationships. According to Eq. (3), $k \propto H^{-1}$ and therefore $n = 2D/\lambda = kD/\pi \propto H^{-1}$, i.e., the oscillations are periodic in the reciprocal of the magnetic field. This is demonstrated in Fig. 8. The deviations of the experimental points from the straight lines at low values of the field are due to the spatial dispersion in the case $\mathbf{H} \parallel \mathbf{k} \parallel C_3$ (Sec. 5), and to the time and spatial dispersions in the case $\mathbf{H} \parallel \mathbf{k} \parallel C_2$ (Sec. 6).

Since the oscillations are periodic, we can determine the absolute value of the wave vector $k = \pi H^{-1}/D\Delta H^{-1}$ and the phase velocity of the waves $v = \omega/k = 2HfD\Delta H^{-1}$. In strong fields, the quantity vH^{-1} is independent of the field and it can be used as a wave characteristic. (Many authors employ the mass density $[NF(m)]^{1/2} = H/2\pi^{1/2}\omega$. This density originates in a calculation of the wave velocity based on the ellipsoidal model of the Fermi surface. Therefore, it seems to be less suitable than the quantity vH^{-1} which can be deduced directly from the experimental results). Table I lists the values of vH^{-1} obtained at ~9 GHz for several directions of H and k.[8]

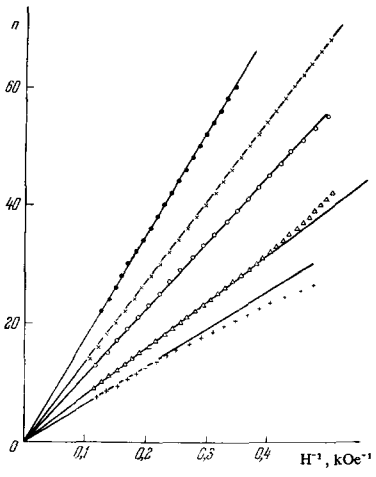

FIG. 8. Dependence of the oscillation order on the reciprocal of the field H^{-1} for some directions of H and k. [15] ●) $\mathbf{H} \parallel C_2$, $\mathbf{k} \parallel C_3$, $\mathbf{E} \parallel C_1$, f = 9.50 GHz, D = 1.74 mm; ×) $\mathbf{H} \parallel C_2$, $\mathbf{k} \parallel C_1$, $\mathbf{E} \parallel C_3$, f = 9.53 HGz, D = 1.74 mm; ○) $\mathbf{H} \parallel C_3$, $\mathbf{k} \parallel C_1$, $\mathbf{E} \parallel C_2$, f = 9.53 GHz, D = 1.74 mm; +) $\mathbf{H} \parallel C_3 \parallel \mathbf{k}$, f = 9.35 GHz, D = 1.00 mm; △) $\mathbf{H} \parallel C_2 \parallel \mathbf{k}$, $\mathbf{E} \parallel C_3$, f = 9.62 GHz, D = 1.00 mm.

Table II. Wave velocities for $\mathbf{H} \parallel \mathbf{k} \parallel C_2$, $\mathbf{E} \parallel C_3$ corresponding to various frequencies

f, GHz	vH^{-1}, 10^{-4} cm/sec	Range of fields	$\frac{\omega}{\Omega}$	$\frac{kv}{\Omega}$	Probable correction for dispersion, %	Reference
~2	2.58	4—25	0.02		<1	9
9.27	2.40±0.1	4—10	0.1	0.1	+1	8
~9	2.40	4—7	0.1	0.1	+1	16
13÷18	2.25 *)					12
21.1	2.36±0.1	4—10	0.2	0.2	+4	8
27.07	2.24±0.1	6—10	0.15	0.1	+3	8
35.86	2.23±0.1	6—10	0.25	0.15	+5	8
52.6	2.30	5—9	0.45	0.4	≈+20	17
	calc.: 2.50±0.1					

*The direction of E given in [12] is evidently incorrect. The cited value of 2.25×10^4 cm/sec refers to the case $\mathbf{E} \parallel C_1$ and the value for $\mathbf{E} \parallel C_3$ should be 2.6×10^4 cm/sec. These values give better agreement with the experimental results for $\mathbf{E} \parallel C_1$.

According to Eq. (3), the phase velocity of the waves should be independent of the frequency. Table II lists the values of vH^{-1} obtained in various investigations for $\mathbf{H} \parallel \mathbf{k} \parallel C_2$, $\mathbf{E} \parallel C_3$. All the values obtained in the frequency range 2—50 GHz are practically identical. A more detailed comparison (for other directions of H, k, and E) is given in[8,18].

It remains to check that the velocity of the P waves is proportional to $\cos\vartheta$ [Eq. (3)]. To do this, we note that the dependence $\cos^{-1}\vartheta$ in the angular diagram is a straight line and therefore the experimental value of H/v for the P waves should fit a straight line perpendicular to the direction of k. Since the crystallographic anisotropy, which becomes manifest when the direction of H is varied, is superimposed on the anisotropy of the P-wave velocity associated with the angle between H and k, the experimental points for H/v in the angular diagram of Fig. 9 fit a straight line only for $\vartheta \gtrsim 30°$. Angular diagrams, similar to those in Fig. 9, are given in[6,8] for other directions of H and k.

Table I presents the results of calculations of the wave velocity, carried out using the ellipsoidal model of the Fermi surface of bismuth. The agreement between the calculated and the measured values of vH^{-1} (within the limits of the experimental error) is evidence of the quantitative agreement between the theory and experiment, and it shows that the ellipsoidal model of the Fermi surface can be used to calculate the wave velocity.

3.3. Damping of Waves

The damping of waves in strong fields is due to relaxation processes, and it can be determined experimentally from the ratio of the amplitudes of the consecutive resonances of the surface impedance of a sample [orders n and (n + 1)]. According to calculations,[5] When $k''D \ll 1$ (i.e., when the damping length is much greater than the thickness of the sample), the resonance value of the surface impedance is

$$Z = \omega^2\tau D/4cn^2\pi^2, \quad (12)$$

i.e., this impedance is proportional to n^{-2}, which is in reasonable agreement with the experimental values (Fig. 3). The value of $\omega\tau$ calculated on the basis of this formula, is ≈40.

In the other limiting cases of $k''D \gg 1$, the ratio of the oscillation amplitudes n_1 and n_2 is $A_1/A_2 = (n_2/n_1)\exp(-\pi\Delta n/\omega\tau)$. Bearing in mind that a modulation method is used in the case of small changes in the pulse amplitude, that the value of $\partial X/\partial H$ or $\partial R/\partial H$ is measured, and that the oscillations are of the form $Z \propto A\sin(H^{-1}/\Delta H^{-1})$, we find that the ratio of the amplitudes of the consecutive oscillations of the derivative (for $\omega\tau \gg 1$) is $A_1'/A_2' = (n_1/n_2)\exp(-\pi\Delta n/\omega\tau)$, and hence $\omega\tau = \pi\Delta n/\ln(n_1A_2'/n_2A_1')$. The results of an analysis of one of the experiments are presented in Fig. 10. The slope of the straight line in that figure gives $\omega\tau = 45$. Values of the same order of magnitude ($\tau \approx 0.5$–0.1 nsec) have been reported in[9,19,20].

Since $k''/k' = 1/2\omega\tau$ (Sec. 1.1), each damping length corresponds to ~100 wavelengths, and therefore such waves can justifiably be regarded as weakly damped.

3.4. Quantum Effects

The Landau quantization, exhibited clearly by bismuth, gives rise to certain features in the wave propagation, which can be divided into two groups: 1) changes in the wave velocity; 2) oscillations of the wave damping.

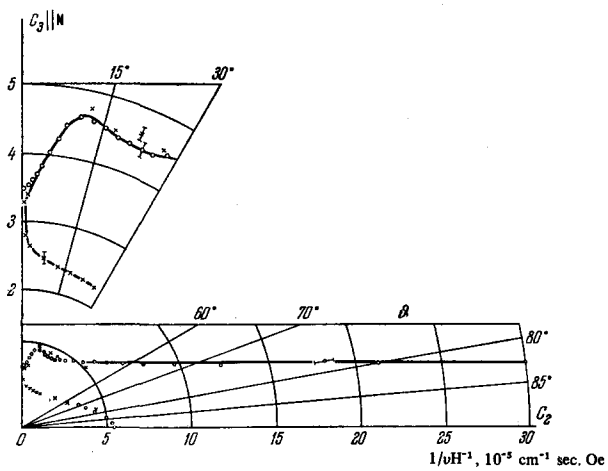

FIG. 9. Dependence of $1/\nu H^{-1}$ on the angle $\vartheta = \sphericalangle(C_3, H)$ for $H \perp C_1$. [8] ●) $E \parallel C_2$; ×) $E \perp C_2$. The experimental errors are shown in the conventional manner. The upper half of the figure shows part of the dependence on a larger scale.

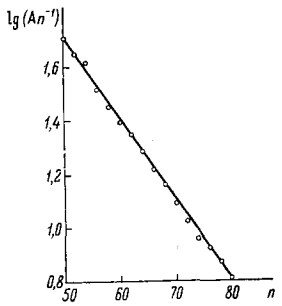

FIG. 10. Dependence of the logarithm of the ratio A/n on n (A is the oscillation amplitude and n is the order of the oscillation). [15] D = 1.74 mm, $H \parallel C_3 \perp k \parallel C_1$, $E \parallel C_2$, f = 9.51 GHz, T = 1.65°K. The slope of the line gives $\omega\tau = 45$.

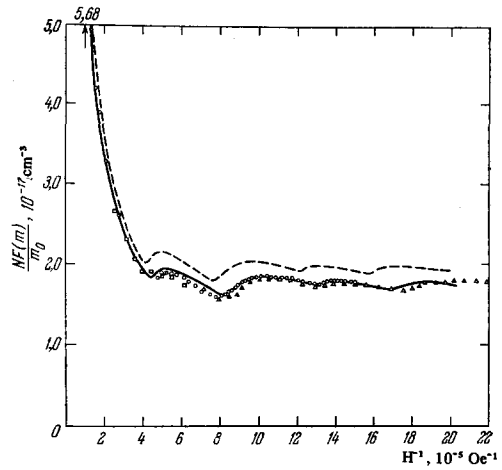

FIG. 11. Dependence of the mass density NF(m) on the reciprocal of the magnetic field. [12] The experimental results are represented by circles, squares, and triangles. The continuous and dashed lines represent calculations based on different parameters of the spectrum of bismuth for $H \parallel k \parallel C_1$, $E \parallel C_2$.

Changes in the wave velocity (i.e., deviations from the dependence $vH^{-1} = \text{const}$) are associated with changes in the Fermi energy and the carrier density, which are caused by an increase in the magnetic field[21] and are observed in fields of only a few kilooersteds.[22] The influence of strong magnetic fields on the wave velocity has been investigated by several workers.[12,23-25] Figure 11 shows the dependence of mass density on the magnetic field for $H \parallel k \parallel C_1$, $E \parallel C_2$.[12] The change in the wave velocity caused by the application of a strong magnetic field can be used to investigate the behavior of bismuth in the ultraquantum limit.

The cause of the quantum oscillations of the damping is evidently the same as that of the Shubnikov-de Haas oscillations, namely, the quantum oscillations of the mean free path of electrons. The presence of oscillations of the wave damping has been mentioned in many papers, for example, in[9,19,23,26]. This effect can be used to measure the absolute amplitude of the oscillations of the mean free path of electrons.[19]

4. TIME DISPERSION

4.1. Hybrid Resonance[27]

The conditions $\omega/\Omega \ll 1$ and $k \cdot v/\Omega \ll 1$ are not satisfied in weak magnetic fields and therefore allowance must be made for the dispersion in time and space. We shall consider the case when $\omega/\Omega \approx 1$ but $k \cdot v/\Omega \ll 1$, i.e., when the spatial dispersion is unimportant. Under these conditions, the wave spectrum can be calculated in a sufficiently general form[2] but since comparisons with the experiments have been carried out only for $k \perp H$,[27] we shall restrict our treatment to this case.

Using the same model as in Sec. 1.1, but bearing in mind the finite value of ω/Ω, we obtain the following expression for the conductivity tensor:[27]

$$\sigma_{xx} = \sigma_{yy} = -i\omega\left(\frac{\omega_{pl\,e}}{\Omega_e^2-\omega^2} + \frac{\omega_{pl\,h}^2}{\Omega_h^2-\omega^2}\right),$$

$$\sigma_{xy} = -\sigma_{yx} = \frac{\omega_{pl\,h}^2}{\omega^2 - \Omega_h^2}\Omega_h - \frac{\omega_{pl\,e}^2}{\omega^2 - \Omega_e^2}\Omega_e, \qquad \sigma_{zz} = i\omega_{pl}^2/\omega, \tag{13}$$

where $\omega_{ple}^2 = Ne^2/m_e$, $\omega_{plh}^2 = Ne^2/m_h$. Solving the dispersion equation, taking account of the equality of the hole and electron densities, and making simple transformations, we obtain the following relationship for a wave polarized perpendicularly to H:

$$k^2 = \frac{4\pi e^2\omega^2}{c}\frac{N(m_e + m_h)}{(\Omega_e\Omega_h - \omega^2)m_e m_h}. \tag{14}$$

We can easily show that if $\omega/\Omega \ll 1$. this expression is identical with the solution given in Eq. (3).

The following conclusions can be drawn from an analysis of Eq. (14).

1) Undamped waves may exist right up to field strengths corresponding to the "hybrid" resonance [$\omega = (\Omega_e\Omega_h)^{1/2}$]. When this field is approached, k increases to infinity if the relaxation time is ignored. The solution near the hybrid resonance point is approximate since the increase in k means that the spatial dispersion has to be allowed for. In particular, the limit of existence of the waves $\omega = \Omega_e - \Omega_h$ is also approximate.

2) If there is no spatial dispersion and the carrier spectrum is quadratic, no singularities are observed in the spectrum of the waves associated with cyclotron resonance. The first-order cyclotron resonance (i.e., when $\Omega = \omega$) is not observed in the surface impedance if there is no spatial dispersion. However, one of the resonances is observed in a field below the hybrid resonance when the spatial dispersion must be allowed for because of the experimental conditions employed (frequency $f \lesssim 100$ GHz).

In the case of bismuth, the situation is more complex than that considered above because there are at least three types of carrier with different masses. For this reason, there are several hybrid resonances and in the intervals between them there is a dielectric anomaly, which is a singularity corresponding to k = 0. In the absence of relaxation processes, this would imply the existence of a uniform high-frequency field in a sample. A typical dependence $k^2(H)$ for three groups of carriers is presented in Fig. 12. We can see that undamped waves ($k^2 > 0$) can exist not only in strong fields but also in regions bounded by a hybrid resonance and a dielectric anomaly. No standing waves have yet been observed in such regions. Table III lists the hybrid resonance and dielectric anomaly fields calculated in[27] for several directions of H and k. The experimental values obtained for f = 70 GHz[27] are in agreement with the theoretical values.

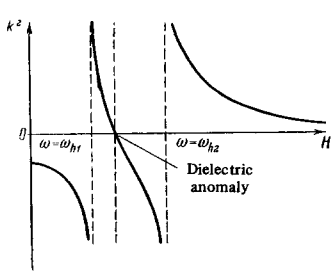

FIG. 12. Schematic representation of the dependence of k^2 on the magnetic field in the presence of two hybrid resonances $\omega = \omega_{h1}$ and $\omega = \omega_{h2}$. [27]

Table III. Hybrid resonance (HR) and dielectric anomaly (DA) fields for H ⊥ k, E ⊥ H and f = 70 GHz, calculated in[27]

Direction of H	Direction of k	H_{HR}, kOe	H_{DA}, kOe
C_3	C_1 C_2	1.45 1.45	—
C_2	C_3 C_1	0.5 5.0 0.5 3.0	0.9 0.95
C_1	C_2 C_3	0.25 0.7 0.25 2.5	—

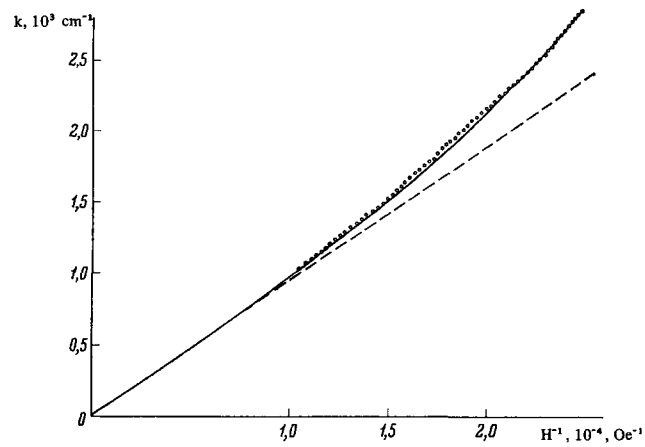

FIG. 13. Dependence of the wave number k on H^{-1} for the P waves. [8] H ⊥ C_3, k ∥ C_2, $\vartheta = 73.5°$, E ∥ C_1, f = 9.50 GHz, D = 1.00 mm. O) Experimental results; the continuous curve represents the calculations based on Eq. (15) and the dashed line is the asymptote.

4.2. Influence of the Time Dispersion on the Spectrum of P Waves

In some cases, the time dispersion may exert a considerable influence on the wave spectrum even when $(\omega/\Omega)^2 \ll 1$. In view of this, we shall consider the behavior of the P waves in the case of low values of $\cos\vartheta$.[8] One of the experimentally obtained dependences $k(H^{-1})$, presented in Fig. 13, deviates considerably from the straight line. In this range, $(\omega/\Omega)^2 \lesssim 3\times 10^{-2}$ and $(k\cdot v/\Omega)^2 \lesssim 10^{-2}$, and we can use the asymptotic values of the components of the conductivity tensor. However, we find that $(\omega \tan\vartheta/\Omega)^2 \approx 0.4$, which means that terms of the $k_y k_z$ type must be included in the dispersion equation. We thus obtain

$$k^2 = \frac{4\pi\omega}{ic^2}\frac{\sigma_{yy}}{\cos^2\vartheta}\left(1 - \frac{\sigma_{yy}\sigma_{zz}}{\cos^2\vartheta}\right)^{-1},$$

which, in the case corresponding to Fig. 13, transforms into

$$k^2 = \frac{4\pi\omega}{ic^2}\frac{\sigma_{33}(1)}{\cos^2\vartheta - (\omega^2/\Omega^2)}. \tag{15}$$

The curve in Fig. 13, on the basis of Eq. (15), is in good agreement with the experimental results.

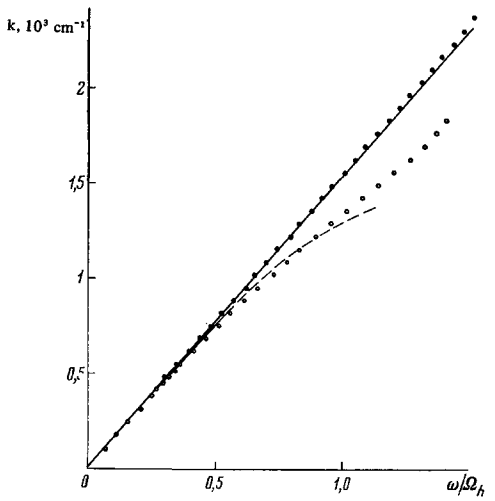

FIG. 14. Dependence of k on the reciprocal of the magnetic field. [15] H ∥ C_1 ⊥ k ∥ C_2, E ∥ C_3, D = 0.47 mm. ○) f = 35.86 GHz; ○) f = 9.35 GHz. The continuous line is the asymptote and the dashed curve represents the calculations based on Eq. (16).

5. SPATIAL DISPERSION

The spatial dispersion is due to the following causes: 1) the finite motion of carriers in a plane perpendicular to the field H (the parameter which determines the wave behavior is the quantity $\mathbf{k}\cdot\mathbf{v}_\perp/\Omega = kR \approx d/\lambda$); 2) the infinite motion of carriers along the field H (the dispersion is associated with those terms of the conductivity tensor which contain $\mathbf{k}\cdot\bar{v}_z/\omega \approx v_{e,h}/v$); 3) the infinite motion of carriers along the field H (the dispersion is associated with those terms of the conductivity tensor which contain $\mathbf{k}\cdot\bar{v}_z/\Omega$); the last case is closely associated with the time dispersion and will be considered in the next chapter.

5.1. Spatial Dispersion for H ⊥ h

If H ⊥ k, the spatial dispersion alters the dependence of the wave velocity on the magnetic field. Some theoretical estimates relating to this case are derived in[28] on the assumption that $\omega/\Omega \ll 1$ but they are not very suitable for bismuth because the conditions $\mathbf{k}\cdot\mathbf{v}_\perp/\Omega \approx 1$ and $\omega/\Omega \ll 1$ can be satisfied simultaneously only at relatively low frequencies (f ≈ 1 GHz). The deviation of the dependence v(H) from linearity was detected experimentally by Khaĭkin et al.[6] Later, similar observations for H ∥ C_1 ⊥ k ∥ C_2 were reported by Lupatkin and Nanney.[29] For this orientation of the vectors H and k the calculations are relatively simple right up to a field H such that $\omega/\Omega_h \approx 1$; in this case, $\omega/\Omega_e \ll 1$ (see Sec. 1.3) and $d_e \ll d_h$. Thus, the contribution of electrons can be described by the asymptotic expression obtained in Sec. 1.4 and the quantities $\sigma_{33}(1)$, $\sigma_{22}(1)$ and $\sigma_{23}(1)$ for holes can be calculated from Eq. (4), in which the terms $\sim(\psi/\Omega)^2 \approx (\mathbf{k}\cdot\mathbf{v}/\Omega)^2$ should be included. If $\omega/\Omega_h = 1$ and f = 36 GHz, we find that $\psi/\Omega \lesssim 0.15$ but if f = 9 GHz, we obtain $\psi/\Omega \lesssim 0.6$ and there is no need to include higher orders of ψ/Ω. Simple but laborious calculations, similar to those carried out in Sec. 1.4, give

$$k^2 = \frac{\omega^2}{H^2}\frac{1}{\pi\hbar^3}\left[\frac{2}{3}(2\varepsilon_h)^{3/2}M_1^2M_3^{1/2} + 6(2\varepsilon_e)^{3/2}m_\alpha^{1/2}m_\beta^{1/2}m_2^{3/2}\right]$$

$$\times\left[1+\frac{2e^2}{\omega^2\pi\hbar^3 c}\frac{\omega^2}{\Omega_h^2}M_1^{-1/2}M_3^{-1/2}(2\varepsilon_h)^{5/2}\left(M_1^{1/2}+\frac{2\omega}{\Omega_h}\frac{M_3^{1/2}}{4-(\omega/\Omega^2)}\right)\right]^{-1}. \quad (16)$$

It follows from Eq. (16) that if $\omega/\Omega \approx 1$ the spatial-dispersion correction of k is proportional to ω^{-2}. At ~9 GHz, this correction amounts to ~15% and at ~36 GHz it is only ~1%. Figure 14 shows the results of the calculation alongside the experimental values. The discrepancy between the theory and experiment in the range $\omega/\Omega_h > 1$ is due to the fact that the higher terms of the expansion of the conductivity tensor have been neglected.

5.2. Landau Damping

The spatial dispersion associated with the drift of carriers along the magnetic field gives rise not only to a dependence of vH^{-1} on the field but also to a strong damping of the waves which occurs if $\mathbf{k}\cdot\bar{v}_z/\omega > 1$. This phenomenon is known as the Landau damping[30] and it imposes restrictions on the possible existence of weakly damped waves. It is shown in[2] that undamped waves cannot exist at all if $\mathbf{k}\cdot\bar{v}_z/\omega \gg 1$. The only exceptions are those cases when H ⊥ k and the direction of the field coincides with the symmetry axis of that part of the Fermi surface for which $\mathbf{k}\cdot\bar{v}_z/\omega > 1$ (but not with the symmetry axis of the whole Fermi surface regarded as an assembly of its separate parts!).[31,32]

The case $\mathbf{k}\cdot\bar{v}_z/\omega \approx 1$ is of interest from the experimental point of view but it cannot be analyzed theoretically in its general form. Therefore, as in Sec. 5.1, we shall consider a specific case, namely, the behavior of waves for H ∥ k ∥ C_3.[31] In this case, the symmetry of the problem is high and all the nondiagonal components of the conductivity tensor vanish in the $(\omega/\Omega)^2 \ll 1$ approximation. The dispersion equation can now be separated into two identical equations

$$i\sigma_\perp = c^2k^2/4\pi\omega,$$

where $\sigma_\perp = \sigma_{11}(3) = \sigma_{22}(3)$. In considering the given problem, we must bear in mind that, according to the estimates obtained experimentally for $\mathbf{k}\cdot\mathbf{v}_F/\omega \approx 1$ (Fig. 15), we have $(\omega/\Omega)^2 \lesssim 0.1$ (in this case, v_F and

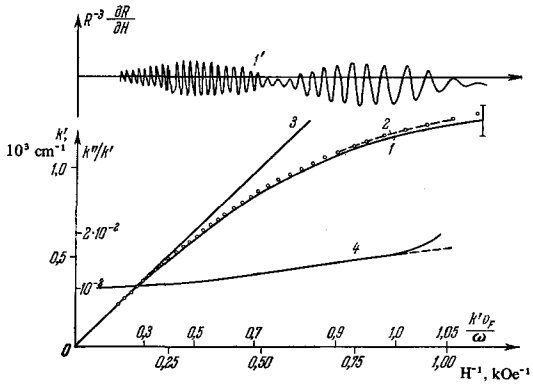

FIG. 15. Wave spectrum in the case of strong spatial dispersion. [31] H ∥ k ∥ C_3, f = 9.35 GHz, D = 1.00 mm. 1) The calculations for $(\omega/\Omega)^2 \ll 1$; 2) the calculations including a correction for time dispersion; 3) asymptote; 4) damping calculated for $\omega\tau = 50$. The vertical segment at the end of curve 1 shows the experimental error. Curve 1' is the experimentally obtained oscillation pattern.

Ω refer to electrons). Using this relationship and Eq. (4), we find that $\sigma_\perp$ differs from the asymptotic value given by Eq. (5) by an additional term of the type:[6]

$$\frac{e^2}{2\pi^2\hbar^3}\int \frac{dp_z m}{\Omega^2}\frac{\overline{(v_\perp\psi)^2}}{i(\omega - k\bar{v}_z)}. \quad (17)$$

Since the field in $\sigma_\perp$ occurs as the factor H^{-2}, it follows that H^{-1} is an explicit function of the parameter $s = \mathbf{k}\cdot\mathbf{v}_F/\omega$. The results of calculations carried out for values of s in the range s = 0–1.05 are given in Fig. 15. The dashed curve in Fig. 15 represents the results of a theoretical calculation carried out using higher terms of the expansion in $(\omega/\Omega)^2$. The agreement between the calculated and the experimental dependences is surprisingly good. We would a priori expect considerable discrepancies because the electron Fermi surface is not ellipsoidal[33] and this is particularly noticeable near the high-symmetry points.

In this case, we must calculate not only the real part k′ but also the imaginary part k″. Introducing the complex quantities $k = k' + ik''$ and $\omega + (i/\tau)$ (instead of ω) into the conductivity tensor and assuming that $k''/k' \ll 1$, $(\omega\tau)^{-1} \ll 1$ (which is justified in the range of fields considered), we can deduce the explicit dependence k″(s) from the dispersion equation; this dependence is shown in Fig. 15 (here, $s = \mathbf{k}'\cdot\mathbf{v}_F/\omega$). When s is increased, the relative damping increases smoothly from $k''/k' = 1/2\omega\tau$ for s = 0 to $\approx 0.8/\omega\tau$ for s = 1. When s is increased still further, an additional Landau damping term must be included. This term is proportional to $\chi^2(s-1)^2$, where χ is the angle of inclination of the electron ellipsoids with respect to the basal plane. Assuming that $\omega\tau = 50$ (see Sec. 3.3), we can easily demonstrate by calculations that for an increase in s from 1 to 1.05 (at this value of s, we have $k''/k' \approx 1/\omega\tau$) the oscillation amplitude for a sample 1 mm thick should decrease by a factor of 3, which is in qualitative agreement with the experimental results (Fig. 15). Under these conditions, the relative amplitude of the impedance oscillations is $\Delta R/R \sim 10^{-2}$.

The solution in the form of an exponentially damped wave, which is assumed in the calculation of the conductivity tensor in[2,6], exists only as long as $k''/k' \ll 1/\omega\tau$. When the two quantities in this expression become comparable, such a solution is no longer valid. This is to be expected because, in the case of strong Landau damping, the field in the interior of a solid-state plasma varies in accordance with a law which is more complex than the exponential dependence[30] and the influence of the boundary of a sample becomes very important. This influence has been ignored in the calculations carried out for an infinite metal. Allowance for the presence of the boundary introduces small corrections, even in the solution which we have obtained for $k''/k' < 1/\omega\tau$.

The behavior of damping in the case $s \gg 1$ can be explained quite satisfactorily. To do this, we shall consider why there is no damping if the carrier orbits have an axis of symmetry. In this case, the electrons which contribute to the Landau damping and which move together with the wave (in a system of coordinates which is associated with the wave) are subject to a constant electric field which is perpendicular to the magnetic field (because the components $\sigma_{z\alpha}$ vanish). The action of this electric field, averaged over a cyclotron period, on an electron-moving along a symmetrical orbit does not result in energy dissipation.

Similar considerations explain also our results for $\mathbf{H} \parallel \mathbf{k} \parallel C_3$. In this case, the electron orbits are inclined to the magnetic field. Obviously, the effect of a spatially nonuniform electric field on electrons moving along such orbits gives rise to a finite Landau damping. Such damping is associated with the inclination of the orbit to the magnetic field because this field is inclined with respect to the axis of the constant-energy ellipsoid. Since the diameter of the orbits of the electrons moving in phase with the wave increases with increasing s (beginning from zero for s = 1), it follows that the damping is zero for electrons which corresponds to a high-symmetry point of the Fermi surface, and which move in phase with the wave (s = 1). The damping gradually increases with increasing s, as found in our calculations.

If the magnetic field is directed at an angle with respect to the wave vector and with respect to the symmetry axes, we find that, when the field is reduced, the Landau damping may appear suddenly at the threshold condition $\mathbf{k}\cdot\mathbf{v}_z/\omega = 1$.[31] This is due to the presence of a relatively small component E_z in the wave. Naturally, this gives rise to finite absorption as soon as s exceeds unity. The range of fields in which the damping rises rapidly can be estimated by postulating that, during the time between two collisions, the phase of the field "seen" by an electron at a high-symmetry point changes by less than π, which gives the relative width $\sim 1/\omega\tau$.

5.3. Measurement of the Electron Velocity in Bismuth

The threshold of the Landau damping is associated with the Fermi statistics of the carriers in a metal. According to these statistics, the velocities of electrons and holes lie within a limited range from $+v_F$ to $-v_F$, where v_F is the maximum drift velocity of the carriers for a given direction of the magnetic field, i.e., it is the velocity at a high-symmetry point of the Fermi surface. In the case of bismuth, it is found that the velocity of the electrons at a high-symmetry point v_{Fe} exceeds the corresponding velocity of holes v_{Fh} for those directions of the field along which the Landau damping has been observed. Thus, the Landau damping threshold is determined by the electron spectrum.

The velocity of a wave corresponding to the Landau damping threshold can be measured experimentally by counting the number of oscillations (starting from $H^{-1} = 0$). In this way, it is possible to measure the electron velocity using the condition $v = v_{Fe}$, which corresponds to the Landau damping threshold. Such measurements have been reported in[13,34].

As in measurements of any other physical quantity, it is necessary to consider the problem of the experimental errors in the determination of the Fermi velocity. If we consider the experimental results presented in Fig. 15, it becomes clear that without additional calculations it is difficult to deduce the electron velocity from such results more accurately than to within ~10%. This is due to the variation of the rela-

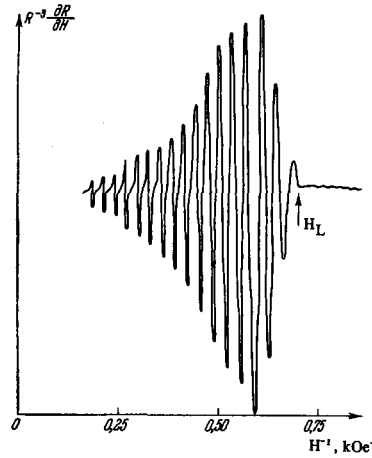

FIG. 16. Oscillations obtained in the determination of the Landau damping threshold H_L. [13] The smooth decrease in the oscillation amplitude with diminishing values of H^{-1} is due to the increasing impedance R. $H \perp C_3$, $k \parallel C_2$, $\vartheta = 57°45'$. $E \parallel C_1$, f = 9.27 GHz, D = 0.47 mm, T = 1.5°K.

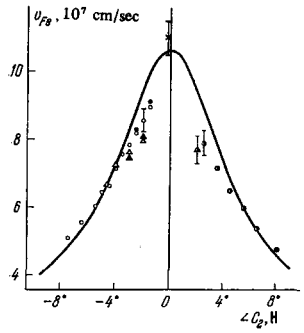

FIG. 17. Determination of the Fermi velocity of electrons in the basal plane. The continuous curve represents the calculations based on the assumed Fermi surface model (the error may be ±5%). The experimental error is given for some of the measurements. $k \parallel C_2$, $H \perp C_3$. ○), ●), ◑) D = 1.00 mm; △), ▲), ◭) D = 0.47 mm; ○), △) $\vartheta < 10°$; ◑), ◭) $60° > \vartheta > 50°$; ●), ▲) $\vartheta > 60°$; X) velocity determined from the cyclotron resonance shifted by the Doppler effect.

tive damping in the range $s < 1$ and the very smooth rise of the damping in the range $s > 1$ (curve 4 in Fig. 15). However, we have pointed out in Sec. 5.2 that the Landau damping can appear suddenly and that this should give rise to an nonmonotonic dependence of the oscillation amplitude on the field (Fig. 16). Khaĭkin and Édel'man[13] gave an experimental criterion which can be used to determine whether the observed threshold of the existence of oscillations does indeed represent the Landau damping threshold. The essence of this criterion is a comparison of the experimental results obtained for samples of various thicknesses and for the same sample along crystallographically equivalent field directions but different orientations of the field relative to the wave vector. The latter technique is particularly convenient if H lies in the basal plane since this makes it possible to compare several experiments carried out on the same sample. If the same value of the velocity is obtained in all these cases (if H is inclined with respect to k, the measured quantity is the projection of v_z along the direction of k), it follows that this value represents the velocity of the electrons at a high-symmetry point. The relative error in these measurements is equal to the reciprocal of the number of oscillations. The results of such an analysis, carried out for $k \parallel C_2$, $H \perp C_3$, are presented in Fig. 17. It follows from this figure that the velocity found experimentally from the Landau damping threshold represents the velocity at a high-symmetry point if $8° \gtrsim \measuredangle(H, C_2) \gtrsim 3°$. However, if $\measuredangle(H, C_2) > 8°$, the oscillation threshold is governed either by the damping of the Doppler-shifted cyclotron resonance (Sec. 6.2) or by the relaxation damping. The velocity in the range $\measuredangle(H, C_2) \lesssim 3°$ can be measured using thicker (>1 mm) samples. The weakening of the Landau damping with decreasing angle $\measuredangle(H, C_2)$ is associated with the absence of damping in the $H \parallel C_2 \parallel k$ case, as discussed in Sec. 5.2.

5.4. Propagation of Electromagnetic Excitations in the Case $k \cdot v_F/\omega > 1$ under Conditions of Strong Landau Damping

We shall consider this problem qualitatively. As demonstrated in Sec. 5.2, the solution in the form of an exponentially damped wave ceases to satisfy the Maxwell and transport equations if $k''/k' \gtrsim 1/\omega\tau$. This can be explained as follows. Consider a wave traveling from the surface of a sample at a phase velocity $v = \omega/k < v_F$. The electric field of this wave disturbs the equilibrium distribution of carriers. Those electrons which move at a velocity $v_F > v$ can "carry" information on the electromagnetic field to a depth equal to the mean free path l in a time interval $\tau \approx l/v_F < l/v$. If the damping length of the wave is less than l (this is ensured by the condition $k''/k' > 1/\omega\tau$), it follows that the field at a distance of the order of l from the surface is determined by the "fast" electrons. In other words, the phase velocity increases with depth in the metal and it approaches the value v_F.

The field distribution in a metal is then similar to that which is observed in the anomalous skin effect. This similarity is to be expected because the high-frequency field distribution in a metal under anomalous skin effect conditions (in the absence of a magnetic field) represents the limiting case ($H \to 0$) of the effects considered here.

These qualitative considerations are supported by the experimental results (Fig. 18). When the Landau damping becomes active, the oscillation amplitude decreases by two orders of magnitude but the oscillations are still observed right up to the Doppler-shifted cyclotron resonance of the electrons (Sec. 6.2). The value of the wave vector averaged over the thickness of the sample can be found by counting a number of oscillations: for the results presented in Fig. 18, we find that $\bar{k} = (1.38 \pm 0.06) \times 10^3$ cm^{-1}. If we know the effective mass[33] and the velocity v_F (determined from the Landau damping threshold in the same trace), we can use the resonance condition $\Omega = \omega + k \cdot v_F$ to calculate the value of the wave vector at the surface $k_S = (1.76 \pm 0.1) \times 10^3$ cm^{-1}. The difference between the values of k and k_S exceeds the experimental error and is in agreement with our qualitative considerations: k decreases away from the surface, i.e., the phase velocity of the wave increases with depth.

6. CYCLOTRON RESONANCE AND SPATIAL DISPERSION

6.1. High-order Cyclotron Resonances

The analysis in Sec. 4 shows that, in the range of magnetic fields in which wave propagation is possible,

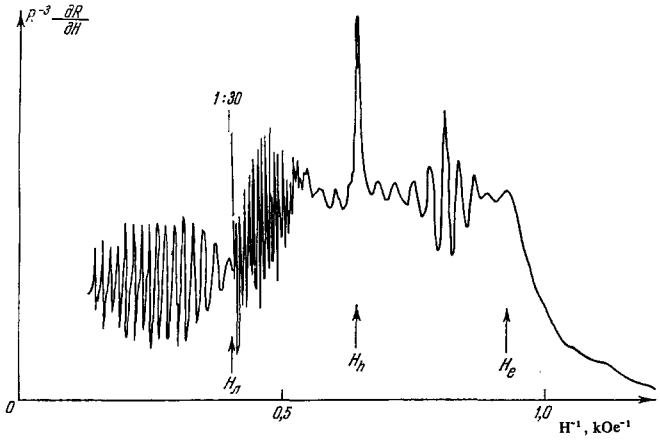

FIG. 18. Oscillations of the surface impedance. [31] $\mathbf{H} \perp C_3 \parallel \mathbf{E}$, $\mathbf{k} \parallel C_2$, $\vartheta = 3°10'$, f = 9.62 GHz, D = 1.00 mm, T = 1.5°K. H_e is the Landau damping threshold; H_e is the Doppler shifted cyclotron resonance of holes, associated with a wave whose polarization in strong fields is close to the direction of the C_1 axis. The short-period oscillations, which can be seen between H_L and H_h, are also associated with this wave. The line denoted by 1:30 shows where the amplification of the system was increased by a factor of 30.

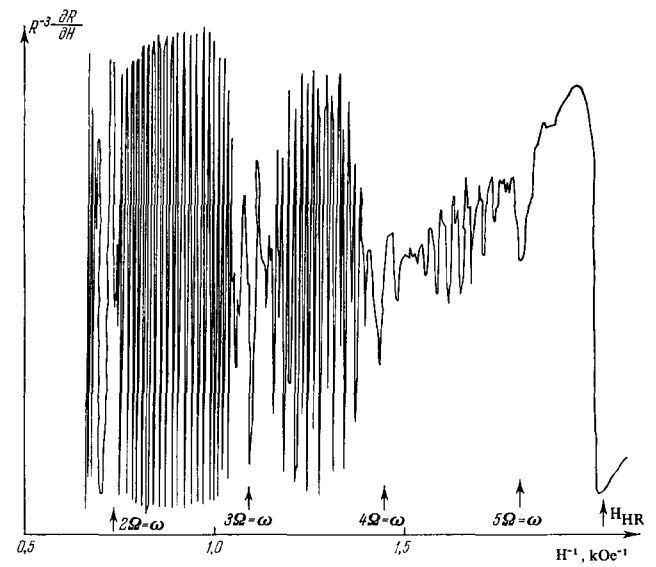

FIG. 19. Oscillations of the surface impedance of bismuth, demonstrating the excitation of higher-order resonances ($n\Omega = \omega$, where n = 2, 3, 4, 5). [15] $\mathbf{H} \parallel C_1 \perp \mathbf{k} \parallel C_2$, $\mathbf{E} \parallel C_3$, f = 35.9 GHz, D = 0.47 mm, T = 1.4°K. H_{HR} is the hybrid resonance field. The arrows denoted by $n\Omega = \omega$ show the values of the field at which the resonance condition is satisfied for holes.

no cyclotron resonance ($\omega/\Omega = 1$) is observed. In some cases, the hybrid resonance field H_{HR} is so low that the fields satisfying the condition $n\Omega = \omega$ for heavier carriers (n = 2, 3, ...) are higher than H_{HR}. This situation occurs, for example, if $\mathbf{H} \parallel C_1$, $\mathbf{k} \parallel C_2$. In This case, $H_{HR} \sim 500$ Oe for ~36 GHz, and in fields exceeding H_{HR}, hole resonances with n = 2, 3, 4, and 5 may occur. It is known that resonances at multiples of the cyclotron frequency appear only in the presence of spatial dispersion[35] and therefore they have not been considered in Sec. 4 (spatial dispersion has been ignored in that section).

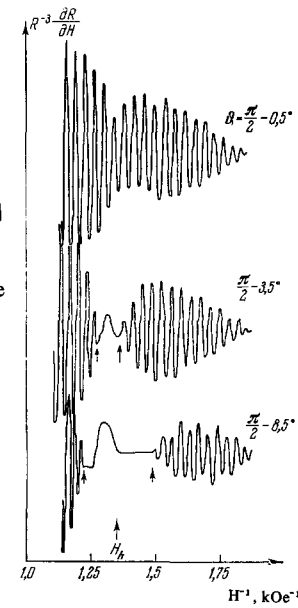

FIG. 20. Oscillations of the surface impedance of bismuth showing the thresholds of the Doppler damping. [13] The arrows show the fields which were regarded as the thresholds in the analysis of the experimental results. H_h is the field obtained by calculation for the first-order cyclotron resonance of holes at a high-symmetry point in the case $\vartheta = \pi/2$. $\mathbf{H} \perp C_3 \parallel \mathbf{E}$, $\mathbf{k} \parallel C_2$, f = 9.62 GHz, D = 1.00 mm, T = 1.5°K.

According to Eq. (4), the conductivity σ_{ik} may exhibit resonances of any order n. In the case of an ellipsoidal Fermi surface, the corresponding resonance terms should be multiplied by $(\psi/\Omega)^{2n}$. This factor represents the spatial dispersion and, because of it, there are no surface impedance resonances if $\psi/\Omega \ll 1$ and τ is finite. However, the condition $\psi/\Omega \ll 1$ can be satisfied only at very high frequencies. For f = 36 GHz and n = 2, we have $\psi/\Omega \approx 0.6$ (this should be compared with $\psi/\Omega \approx 0.15$ for n = 1, as shown in Sec. 5.1). This inhomogeneity of the high-frequency field makes it possible to observe cyclotron resonance in bismuth at high frequencies.[36] Investigations of the wave spectra show that the excitation of higher-order resonances alters the wave velocity, causes strong damping of the waves, and suppresses oscillations of the surface impedance of a plane-parallel plate. Moreover, cyclotron resonance (Fig. 19) is observed in the surface impedance of semi-infinite bismuth samples (the results presented in Fig. 19 should be interpreted in the knowledge that under strong damping conditions a sample may be regarded as infinitely thick).

6.2. Cyclotron Resonance at Frequencies Shifted by the Doppler Effect

We shall now consider the influence of cyclotron resonance on the wave spectrum in the case defined by $\vartheta = \sphericalangle(\mathbf{H}, \mathbf{k}) \neq \pi/2$. The drift of carriers along the vector k makes the carriers "see" an external field of frequency $\omega - \mathbf{k} \cdot \bar{\mathbf{v}}_z$ because of the Doppler effect. The cyclotron resonance condition is now $n\Omega = \omega - \mathbf{k} \cdot \bar{\mathbf{v}}_z$. The value of $\bar{v}_z$ for the group of carriers considered ranges from $-v_F$ to $+v_F$ because they obey the Fermi statistics. Therefore, at any point in the range of fields given by the condition[13]

$$n\Omega_{1n} = \omega + k(H_{1,n})\, v_F \cos\vartheta, \quad n\Omega_{2n} = \omega - k(H_{2,n})\, v_F \cos\vartheta, \qquad (18)$$

there are carriers which satisfy the resonance condition.

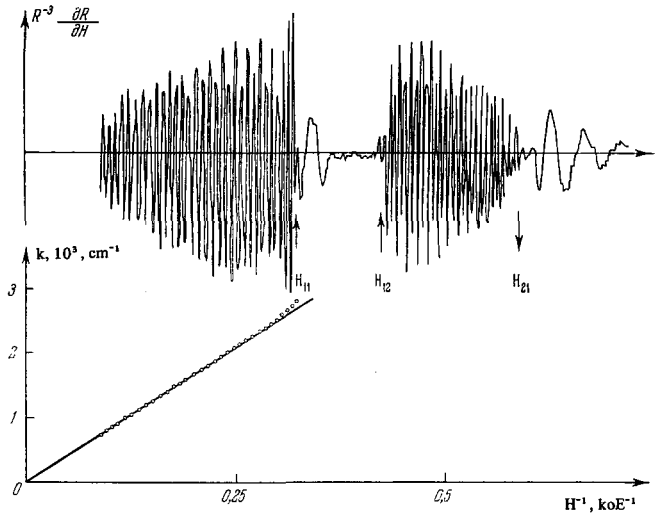

FIG. 21. Oscillation pattern used in the determination of the Doppler damping thresholds H_{11}, H_{12}, and H_{21}. [15] $\mathbf{k} \parallel C_2$, $\mathbf{H} \perp C_3 \parallel \mathbf{E}$, $\vartheta = 66°$, f = 35.9 GHz, D = 1.00 mm.

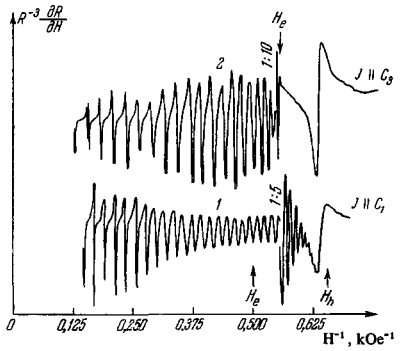

FIG. 22. Oscillation pattern used in determination of the Doppler damping thresholds for holes H_h (curve 1) and electrons H_e (curve 2). [13] The arrow H_e against curve 1 shows the calculated damping field for the electrons represented by this curve. $\mathbf{H} \parallel \mathbf{k} \parallel C_2$, f = 9.27 GHz, D = 0.47 mm, T = 1.5°K. The lines denoted by 1:5 and 1:10 mark the points at which the amplification was increased.

Using Eq. (4) we can show that, when the field lies in the interval defined by Eq. (18), the components σ_{ik} should have imaginary and real parts (even when $\omega\tau \to \infty$), which should give rise to the damping of waves.

The appearance of damping can be observed most easily by recording the oscillations for various values of the angle ϑ, beginning from $\vartheta = \pi/2$. In this way, we can observe a region of strong damping which broadens when the angle ϑ is reduced because of the increase in the projection of $\mathbf{v}_F$ on $\mathbf{k}$ (Fig. 20). Similar behavior can also be observed near higher-order resonances (Fig. 21).

When the angle ϑ is reduced, the threshold H_{21} shifts in the direction of weaker fields in which oscillations of the surface impedance usually disappear (this is due to strong relaxation damping, Landau damping, higher-order resonances, hybrid resonance, etc.). The damping threshold H_{11} and the associated resonance at a frequency shifted by the Doppler effect can be observed also when $\vartheta = 0$.[13,16] This phenomenon has been considered theoretically in[37]

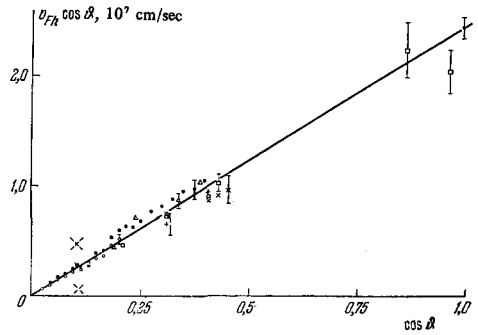

FIG. 23. Determination of the Fermi velocity v_{Fh} and the effective mass m_h of holes located at a high-symmetry point. Basal plane, $\mathbf{H} \perp C_3$, $\mathbf{k} \parallel C_2$. [15] The straight line is plotted using the value $v_{Fh} = 2.46 \times 10^7$ cm/sec obtained for $\vartheta = 0$. ○), □) $v_{Fh}\cos\vartheta$ calculated from Eq. (19); +) calculated using Eq. (20) and n = 2; the other symbols represent the calculations based on Eq. (20); X) calculated assuming $m_h = 0.218m_0$; X) calculated assuming $m_h = 0.212m_0$; ●), ○) f = 9.62 GHz, D = 1.00 mm; △) f = 9.27 GHz, D = 0.47 mm. The other symbols represent the values for f = 35.86 GHz, D = 0.47 mm. The vertical segments near some points represent the experimental errors.

The threshold of the resonance damping of waves is observed clearly if the field H_{11} is greater than the field corresponding to the Landau damping threshold or if there is no Landau damping, which occurs—for example—when $\mathbf{H} \parallel \mathbf{k} \parallel C_2$ irrespective of the wave polarization (Sec. 5.2). Oscillations recorded in this case for $\mathbf{E} \parallel C_1$ and $\mathbf{E} \parallel C_3$ are shown in Fig. 22. The wave spectrum for $\mathbf{E} \parallel C_3$ is governed mainly by electrons and therefore oscillations stop when the electron resonance conditions are reached. A weak-field peak in Fig. 22 represents a hole resonance for a wave polarized in strong fields along C_1; this resonance appears for any polarization of E because the wave polarization near resonance is elliptical. If $\mathbf{E} \parallel C_1$, the wave spectrum is determined by holes and its threshold is found at the hole resonance field. In this case, the electron resonance, which occurs in a higher field, has no influence on the wave spectrum.

As demonstrated in Sec. 5.4, even the waves subject to the Landau damping may exhibit cyclotron resonance at a frequency shifted by the Doppler effect.

6.3. Measurement of the Hole and Electron Velocities

Cyclotron resonance shifted by the Doppler effect can be used to measure the velocity of carriers at a high-symmetry point of the Fermi surface because the effective masses can be calculated from the cyclotron resonance data.[33] According to our cyclotron resonance measurements, the hole Fermi surface has an axial symmetry to within ~0.1%. Therefore, if we collect the results of all the measurements of the hole resonance for $\mathbf{H} \perp C_3$ and use the formula

$$v_{Fh}\cos\vartheta = \frac{e}{m_h c}\frac{H_{11}-H_{12}}{k_{11}-k_{12}} \qquad (19)$$

(it is assumed that both thresholds are observed and the splitting is weak, so that k_{12} can be found by extrapolation[13,34]) or the formula

$$v_{Fh}\cos\vartheta = (\Omega_h - \omega)/k_{11}, \qquad (20)$$

and then plot the results obtained using the coordinates $v_{Fh}\cos\vartheta$ and $\cos\vartheta$, we find that all the points fit a

Table IV. Fermi velocities of carriers in bismuth

	v_F (exper.), 10^{-7} cm/sec^{-1}	v_F (calc.), 10^{-7} cm/sec^{-1}	Reference
$H \perp C_3$	Holes 2.46±0.1	2.55±0.15	15
	2.53	2.55±0.15	38
$H \parallel C_2$	Electrons 11.0±0.5	10 6±0.5	15
$H \parallel \beta$ axis of electron ellipsoid	7.4±0.4	7.4±0.3	15

single straight line (Fig. 23), provided the value of m_h is suitably selected.* The values found in this way are: $v_{Fh} = (2.46 \pm 0.1) \times 10^7$ cm/sec and $m_h = 0.215\ m_0$.

Since a reliable value is available for the electron mass at a high-symmetry point,[33] we can determine v_{Fe} from Eq. (20) and from the experimentally recorded traces of the type shown in Fig. 22. The carrier velocities reported in[15,38] are listed in Table IV.

As in the determination of the carrier velocity from the Landau damping threshold (Sec. 5.3), we have to consider the accuracy of the measurements which is related to the need to calculate the spectrum. This problem demands laborious calculations and it has been solved only for the $H \parallel k \parallel C_1$ case.[38] The results of the calculations of the damping are given in Fig. 24, together with the values obtained experimentally and reported in[38].

The accuracy of the determination of the carrier velocity in other cases can be found by estimating the damping near the threshold. Thus, when $\vartheta \approx \pi/2$, $H \perp C_3$, $k \parallel C_2$ near the damping threshold[15]

$$k''/k' \approx (3/4\pi)\frac{\Omega-\omega}{\omega} \times \left[1-\frac{\Omega-\omega}{kv_{Fh}\cos\vartheta}\right].$$

At the point $\Omega = \omega + kv_{Fh}\cos\vartheta$, the ratio given by the above expression vanishes and this results in the "pulling" of the oscillations into the resonance region. We shall assume that oscillations can be observed if $\sim 10^{-4}$ of the incident wave power returns to the investigated surface after reflection from the opposite surface of a slab (this is equivalent to a sensitivity $\Delta R/R \approx 10^{-4}$). Then, the damping length for a sample $D = 1$ mm thick should be ~ 0.5 mm, i.e., $k'' \approx 20$ cm^{-1}. Since $k' \approx 10^3$ cm^{-1}, it follows that $k''/k' \approx 2\%$. Such damping is reached at $\vartheta = 80°$, $f = 9.6$ GHz when we move away from the damping threshold by $\sim 5\%$ of the width of the damping region. Under these conditions, the error in the determination of the difference $H_{11} - H_{12}$ may be of the same order of magnitude ($\sim 5\%$).

The problem of the exact calculation of the wave spectrum presents not only computational but also fundamental difficulties. As in the case of the Landau damping, we may encounter a situation in which a wave at the surface of a sample is damped out in a distance

*The value of m_h must be selected because cyclotron resonance investigations do not yield the value of the hole mass at a high-symmetry point. [33]

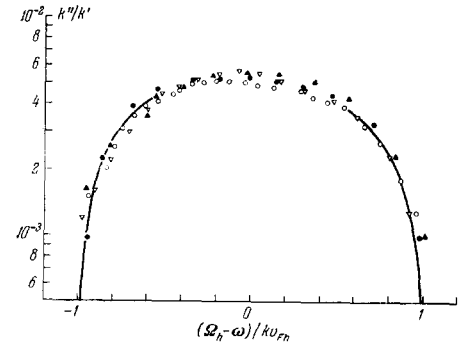

FIG. 24. Dependence of the resonance damping k''/k' on $(\Omega_h-\omega)/kv_{Fh}$. [38] $H \parallel k \parallel C_1$, $E \parallel C_2$, f = 51.0 GHz. The continuous curve represents the calculated values and the separate points plot the experimental results obtained for samples of different thicknesses in the range ~0.8-3 mm.

shorter than the mean free path of carriers and then the distribution of the field in the sample is similar to that considered in Sec. 5.4.

7. CYCLOTRON WAVES

Dispersion in time and space is responsible not only for the waves in a compensated metal, which we have just considered, but also for waves of a different type, which are known as cyclotron waves. This name is used to indicate that the appearance of such waves is associated with cyclotron resonance. Cyclotron waves may exist in any metal. They have been observed experimentally in bismuth[39,40,41] and in alkali metals.[42,43]

We shall be interested in "ordinary" cyclotron waves in which the field E is parallel to an external magnetic field H. If the field directions are symmetrical (for example, $H \parallel C_1$ or $H \parallel C_2$), the spectrum of the cyclotron waves for $k \perp H$ is given by the equation $\sigma_{zz} + (ic^2k^2/4\pi\omega) = 0$, where the component σ_{zz} of the conductivity tensor is defined by Eq. (4).

If the magnetic field is strong so that $\omega/\Omega \gg 1$, the inequality $\mathrm{Im}\,\sigma_{zz} > 0$ is satisfied and the propagation of undampled waves is impossible. If the magnetic field is such that $\omega/\Omega \approx 1$ for any of the carrier groups, we find that the terms with $n = 1$ play an important role and[40]

$$\sigma_{zz} = \sigma^0_{zz} - \frac{ie^2}{2\pi^2\hbar^3}\int_{-p_{z_0}}^{p_{z_0}} dp_z \frac{m\omega}{\Omega^2}\frac{P(\psi^2)}{1-(\omega/\Omega)^2} \qquad (21)$$

where the polynomial $P(\psi^2)$ is positive (its form depends on the shape of the Fermi surface and on the direction of H) and σ^0_{zz} is a slowly varying function of k and H, which contains all the other terms (its value differs little from σ_{zz} for $H \to \infty$). It follows from Eq. (21) that if $1 \gg [1 - (\omega/\Omega)^2] > 0$, we have $\mathrm{Im}\,\sigma_{zz} < 0$, which means that undamped waves may be propagated. In general, when the field is directed at an angle with respect to the symmetry axis of the resonating Fermi surface (cyclotron waves of type I), the polynomial $P(\psi^2)$ begins with a constant and the zero value of k is not reached at resonance but at a higher value of the field corresponding to a dielectric anomaly[27] and the value of k increases with decreasing field. Waves with small values of k do not exist

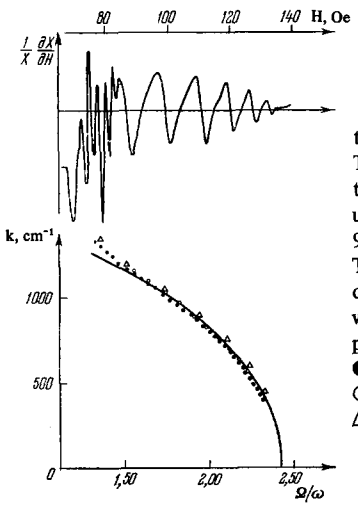

FIG. 25. Cyclotron wave spectrum for $k \parallel C_3$, $H \parallel E \parallel C_1$. [40] The upper part of the figure shows the trace obtained experimentally under the following conditions: f = 9.80 GHz, D = 0.21 mm, T = 1.5°K. The lower part of the figure is the dependence of k on Ω/ω at low values of k (corresponding to long-period oscillations in the trace). ●) f = 9.60 GHz, D = 1.00 mm; ○) f = 9.51 GHz, D = 0.47 mm; △) f = 9.80 GHz, D = 0.21 mm.

near resonance. However, if the field is parallel to the symmetry axis of the resonating Fermi surface (cyclotron waves of type II), the polynomial $P(\psi^2)$ begins with a quadratic term, which corresponds to the wave spectrum $k^2 \propto [1 - (\omega/\Omega)^2]$ for $\psi^2 \ll 1$, $1/[1 - (\omega/\Omega)^2] \gg 0$. The calculations reported in[42] show that, for a given value of H and ω, type II cyclotron waves may have several different values of k. Obviously, this is possible also in the case of type I waves because the difference between the two cases considered exists only at low values of k.

Waves of type I, associated with the excitation of the cyclotron resonance of electrons of 0.0162 m_0 mass (electrons of two ellipsoids resonate simultaneously), were reported in[39-41]. These cyclotron waves were observed in samples 0.2–1 mm thick, at 1.5–4.2°K and ~9.6 GHz. Two series of oscillations were observed simultaneously (Fig. 25) in one of the samples (0.21 mm thick). A comparison with the measurements of the transparency of bismuth in the cyclotron wave region[41] established that each of the oscillations series in Fig. 25 represented a change (by unity) in the number of half-waves (and not complete waves, Sec. 2.2) which could be fitted into the thickness of the sample.

Standing cyclotron waves of type II were observed only in a sample 0.2 mm thick, at 0.6°K (this temperature was reached by pumping He^3 vapor) and 19.1 GHz.[40] The field $H \parallel C_2$ and the waves were associated with the resonance of that electron ellipsoid whose major axis was perpendicular to the C_2 axis. The spectrum obtained in this case is shown in Fig. 26.

The initial part of the cyclotron wave spectrum (for small values of ψ) was calculated for case I, using the ellipsoidal model of the Fermi surface. The calculation was carried out up to terms $\sim\psi^6$ and the results are presented in Fig. 25. The approximation used was insufficient to calculate the upper part of the spectrum (corresponding to more frequent oscillations in Fig. 25) and this calculation was not attempted.

The spectrum of waves for the $H \parallel C_2$ case was calculated using, as a first approximation, the same ellipsoidal model. However, the value of Ω/ω was not calculated from the values of the field given by the model but from an experimentally obtained trace. The

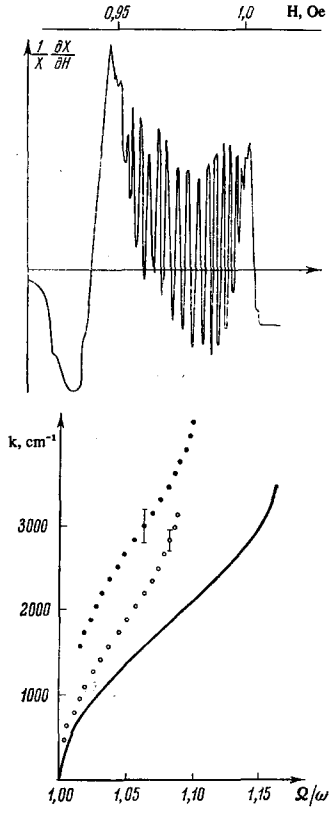

FIG. 26. Cyclotron wave spectrum for $k \parallel C_3$, $H \parallel E \parallel C_2$, f = 19.1 GHz. [40] The upper part of the figure shows the experimentally obtained trace for D = 0.20 mm, T = 0.85°K. The lower part shows the dependence of k on Ω/ω: ●) cyclotron resonance field assumed to correspond to zero value of $\partial X/\partial H$; ○) cyclotron resonance assumed to correspond to maximum of $\partial X/\partial H$; the continuous curve is the calculated dependence.

difference was very considerable because the mass of electrons at a high-symmetry point $m_{hs} = 0.137\ m_0$[33] was larger than the mass corresponding to the central section $m_e = 0.12\ m_0$ used in the determination of the parameters of the model. Figure 26 shows the results of a comparison of the experimental and calculated spectra. The different symbols used in this figure represent different selections of the point corresponding to exact resonance in the experimentally obtained trace. The absolute value of k was found by extrapolation of the initial region near resonance in accordance with the law $k^2 \propto [1 - (\omega/\Omega)^2]$.

In contrast to Fig. 25, the measured and calculated values of k shown in Fig. 26 differ considerably in the quantitative sense and a similar difference is observed for the range of fields in which wave propagation is possible. This difference is primarily due to the nonquadratic nature of the electron spectrum[33] but it deserves further study.

No cyclotron waves associated with the resonance of the hole surface have yet been observed. According to estimates, the relative width of the range of existence of these waves, $\Delta H/H$, should not exceed ~0.5% for $k \parallel C_3$ and, obviously, such waves could not be observed for values of $\omega\tau = 200-300$ for holes (these values were typical of the better samples at 0.6°K at 19 GHz).

It is demonstrated in[44] that an allowance for cyclotron waves is essential in studies of the line profile of cyclotron resonance in bismuth.

8. POSSIBLE FUTURE INVESTIGATIONS OF WAVES

Our review shows that the numerous investigations of the properties of electromagnetic waves in bismuth

have established the characteristic features of this phenomenon and shown their relationship to many other effects (cyclotron resonance, quantum oscillations, surface quantum levels[14]) by describing their properties on the basis of a model of the Fermi surface. Thus, bismuth is a metal whose dynamic carrier properties are not investigated simply for their own sake but can be used to analyze a wide range of phenomena associated with the propagation of waves. These phenomena include the Landau damping, cyclotron resonance at frequencies shifted by the Doppler effect, and cyclotron waves. In its turn, the study of these phenomena has made it possible to refine several of the parameters of the energy spectrum of bismuth. In this way, the behavior of a compensated metal in magnetic and electromagnetic fields have been investigated sufficiently thoroughly to provide a basis for further studies of the wave propagation as a means of determining the carrier energy spectra of other semimetals, especially antimony and graphite. There have been reports of magnetoplasma waves in these two semimetals.[45,46] However, methodological difficulties associated with the preparation of high-quality single crystals and with the need to work in strong fields (because of the lower velocity of waves in antimony and graphite) have impeded detailed studies of plasma phenomena in these semimetals. On the other hand, the electron energy spectra of antimony and graphite are known quite well and therefore investigations of wave propagation can give only some additional detailed data which are not needed very urgently.

In view of this, it would seem much more interesting to use magnetoplasma waves in investigations of alloys because conventional methods (for example, the de Haas-van Alphen effect[47]) yield very limited information on the carrier dynamics in these materials.

It may also be of some interest to study relaxation processes by measuring the damping of waves (such investigations have been started recently[19,20]). This applies, in particular, to studies of the electron-phonon interaction. The same method may be used to determine independently the relaxation times of electrons and holes in bismuth because there are directions of H and E for which the wave spectrum is governed either only by holes or only by electrons of one ellipsoid of the Fermi surface.

Investigations of the nonlinear effects associated with the propagation of waves in bismuth, such as detection[48] and mixing[49] of oscillations, also seem very promising. Hardly any work has been done on this subject and one may expect that new effects will be discovered.

LIST OF SYMBOLS

C_1, C_2, C_3—bisector, binary, and trigonal axes of crystalline bismuth (only 1, 2, and 3 are used in subscripts)

D—thickness of a sample

$d = 2pc/eH$—orbit diameter

E—electric field vector of waves

e—subscript referring to electrons

f—wave frequency

H—static magnetic field

h—subscript referring to holes

j—current density

$k = k' + ik''$—wave vector

l—mean free path of carriers

M_1, M_2, M_3—components of the hole-mass tensor

m—effective mass of carriers

m_0—free-electron mass

m_2, m_α, m_β—components of the electron-mass tensor along principal axes

N—normal to the surface of a sample

N—carrier density

P—subscript referring to waves polarized in strong fields in the (z, y) plane

P—electron (hole) momentum

r—radius vector

S—subscript referring to waves polarized in strong fields perpendicularly to the (z, y) plane

$s = k \cdot \bar{v}_z / \omega$

v—electron (hole) velocity

v—phase velocity of waves or—with a subscript-carrier velocity

x, y, z—coordinate axes; z axis always directed along H; k located in the (z, y) plane

ΔH^{-1}—oscillation period in terms of reciprocal field

δ_{lk}—Kronecker's delta

ϵ—Fermi energy

$\vartheta = \sphericalangle(H, k)$

$\lambda = 2\pi/k$—wavelength

$\sigma_{ik}(l)$—conductivity tensor (l is the direction of the magnetic field)

τ—time between two successive collisions

$\varphi = eHt/mc$—angle in momentum space

$\bar{(\ )}$—averaging over φ

χ—angle of inclination of the major (α) axis of ellipsoid with respect to basal plane

$\psi = \int^{\varphi} (k \cdot v - k_z \bar{v}_z) d\varphi$

$\Omega = eH/mc$—cyclotron frequency

$\omega = 2\pi f$—angular frequency

ω_{pl}—plasma frequency

[1] S. J. Buchsbaum and J. K. Galt, Phys. Fluids 4, 1514 (1961).

[2] É. A. Kaner and V. G. Skobov, Usp. Fiz. Nauk 89, 367 (1966) [Sov. Phys.-Usp. 9, 480 (1967)]; Advan. Phys. 17, 605 (1968).

[3] L. D. Landau and E. M. Lifshitz, Élektrodinamika sploshnykh sred (Electrodynamics of Continuous Media), Fizmatgiz, M., 1959, p. 276; transl. publ. by Pergamon Press, Oxford, 1960.

[4] J. M. Luttinger, Phys. Rev. 119, 1153 (1960).

[5] L. A. Fal'kovskiĭ, Zh. Eksp. Teor. Fiz. 46, 1820 (1964) [Sov. Phys.-JETP 19, 1226 (1964)].

[6] M. S. Khaĭkin, L. A. Fal'kovskiĭ, V. S. Édel'man, and R. T. Mina, Zh. Eksp. Teor. Fiz. 45, 1704 (1963) [Sov. Phys.-JETP 18, 1167 (1964)].

[7] L. A. Fal'kovskiĭ, Usp. Fiz. Nauk 94, 3 (1968) [Sov. Phys.-Usp. 11, 1 (1968)].

[8] V. S. Édel'man, Zh. Eksp. Teor. Fiz. 54, 1726 (1968) [Sov. Phys.-JETP 27, 927 (1968)].

[9] D. S. McLachlan, Phys. Rev. 147, 368 (1966).

[10]D. L. Carter and J. C. Picard, Solid State Commun. 5, 719 (1967).
[11]M. S. Khaĭkin, Prib. Tekh. Eksp. No. 3, 95 (1961).
[12]G. A. Williams and G. E. Smith, IBM J. Res. Develop. 8, 276 (1964).
[13]M. S. Khaĭkin and V. S. Édel'man, Zh. Eksp. Teor. Fiz. 49, 1695 (1965) [Sov. Phys.-JETP 22, 1159 (1966)].
[14]M. S. Khaĭkin, Usp. Fiz. Nauk 96, 409 (1968) [Sov. Phys.-Usp. 11, 785 (1969)].
[15]V. S. Édel'man, Dissertatsiya (Dissertation), IFP AN SSSR, M., 1967.
[16]J. Kirsch, Phys. Rev. 133, A1390 (1964).
[17]B. W. Faughnan, J. Phys. Soc. Jap. 20, 574 (1965).
[18]R. T. Isaacson and G. A. Williams, Phys. Rev. 177, 738 (1969).
[19]R. T. Isaacson and G. A. Williams, Phys. Rev. Lett. 22, 26 (1969).
[20]E. H. Marston and Y. H. Kao, Phys. Kondens. Mater. 9, 195 (1969).
[21]G. E. Smith, G. A. Baraff, and J. M. Rowell, Phys. Rev. 135, A1118 (1964).
[22]L. N. Pelikh and V. V. Eremenko, Zh. Eksp. Teor. Fiz. 52, 885 (1967) [Sov. Phys.-JETP 25, 582 (1967)].
[23]C. Guthmann and A. Libchaber, C. R. Acad. Sci. B 265, 319 (1967).
[24]S. Takano and H. Kawamura, Phys. Lett. A 26, 187 (1968).
[25]D. L. Carter, Phys. Lett. A 27, 679 (1968).
[26]H. Kawamura, S. Nagata, T. Nakama, and S. Takano, Phys. Lett. 15, 111 (1965).
[27]G. E. Smith, L. C. Hebel, and S. J. Buchsbaum, Phys. Rev. 129, 154 (1963).
[28]I. Yokota, J. Phys. Soc. Jap. 21, 1851 (1966).
[29]W. L. Lupatkin and C. A. Nanney, Phys. Rev. Lett. 20, 212 (1968).
[30]L. D. Landau, Zh. Eksp. Teor. Fiz. 16, 574 (1946).
[31]V. S. Édel'man, Zh. Eksp. Teor. Fiz. 56, 25 (1969) [Sov. Phys.-JETP 29, 13 (1969)].
[32]É. A. Kaner and V. G. Skobov, Phys. Lett. A 25, 105 (1967).
[33]V. S. Édel'man and M. S. Khaikin, Zh. Eksp. Teor. Fiz. 49, 107 (1965) [Sov. Phys.-JETP 22, 77 (1966)].
[34]V. S. Édel'man and V. Kamberski, Proc. Tenth Intern. Conf. on Low Temp. Physics, Moscow, 1966, Vol. 3, publ. by VINITI, M., 1967, p. 206.
[35]M. Ya. Azbel' and É. A. Kaner, Zh. Eksp. Teor. Fiz. 32, 896 (1957) [Sov. Phys.-JETP 5, 730 (1957)].
[36]L. C. Hebel, Phys. Rev. 138, A1641 (1965).
[37]P. B. Miller and R. R. Haering, Phys. Rev. 128, 126 (1962).
[38]S. Nagata and H. Kawamura, J. Phys. Soc. Jap. 24, 480 (1968).
[39]V. S. Édel'man and M. S. Khaĭkin, Zh. Eksp. Teor. Fiz. 45, 826 (1963) [Sov. Phys.-JETP 18, 566 (1964)].
[40]V. S. Édel'man, ZhETF Pis. Red. 9, 302 (1969) [JETP Lett. 9, 177 (1969)].
[41]A. Libshaber and J. P. d'Haenens, private communication.
[42]P. M. Platzman, W. M. Walsh, Jr., and E-Ni Foo, Phys. Rev. 172, 689 (1968).
[43]W. M. Walsh, Jr. and P. M. Platzman, Proc. Tenth Intern. Conf. on Low Temp. Physics, Moscow, 1966, Vol. 3, publ. by VINITI, M., 1967, p. 214.
[44]N. B. Brovtsyna and V. G. Skobov, Zh. Eksp. Teor. Fiz. 56, 694 (1969) [Sov. Phys.-JETP 29, 379 (1969)].
[45]G. A. Williams, Bull. Amer. Phys. Soc. 8, 353 (1963).
[46]M. Surma, J. K. Furdyna, and H. C. Praddaude, Phys. Rev. Lett. 13, 710 (1964).
[47]N. B. Brandt, L. G. Lyubutina, and N. A. Kryukova, Zh. Eksp. Teor. Fiz. 53, 134 (1967) [Sov. Phys.-JETP 26, 93 (1968)].
[48]S. J. Buchsbaum and G. E. Smith, Phys. Rev. Lett. 9, 342 (1962).
[49]W. R. Wisseman and R. T. Bate, Bull. Amer. Phys. Soc. 13, 437 (1968).

Translated by A. Tybulewicz